Available online at www.sciencedirect.com

SCIENCE DIRECT®

PERGAMON

International Journal of Multiphase Flow 29 (2003) 675–699

International Journal of Multiphase Flow

www.elsevier.com/locate/ijmulflow

Analysis of collision effects for turbulent gas–particle flow in a horizontal channel: Part I. Particle transport

M. Sommerfeld *

Institut für Verfahrenstechnik, Fachbereich Ingenieurwissenschaften, Martin-Luther-Universität Halle-Wittenberg, D-06099 Halle (Saale), Germany

Received 21 August 2002; received in revised form 29 January 2003

Abstract

The behaviour of spherical solid particles in a horizontal channel flow is analysed using numerical calculations based on the Lagrangian approach. Recent developments in modelling particle motion, wall collisions, wall roughness, and inter-particle collisions are accounted for. The wall roughness model relies on the assumption that the impact angle is composed of the particle trajectory angle and a stochastic component due to wall roughness. A stochastic approach is used to describe inter-particle collisions between the considered particle and a fictitious collision partner which is a representative of the local particle phase. Then the collision probability is calculated on the basis of kinetic theory of gases, but accounting for the velocity correlation of colliding particles in turbulent flows. In order to allow an analysis of wall collisions and inter-particle collisions independent of the effect of particles on the flow, two-way coupling was neglected and flow and turbulence were prescribed. The particle behaviour for different boundary conditions, such as particle size, wall roughness and mass loading is discussed in detail. It is demonstrated that both effects, i.e. wall roughness and inter-particle collisions have a dramatic influence on the particle behaviour in a horizontal channel and the particle phase properties of the developed flow. In order to characterise the particle behaviour, the mean free path between wall collisions is introduced. In a second part of this work integral properties are presented in order to reveal the effects of wall roughness and inter-particle collisions. Moreover, the effect of channel height on the particle phase properties is analysed. Finally, the calculations are compared with detailed measurements by phase-Doppler anemometry in a horizontal channel with a height of 35 mm and a length of 6 m for validation.

Keywords: Gas–particle flow; Horizontal channel; Lagrangian particle tracking; Wall collisions; Wall roughness; Inter-particle collisions

* Tel.: +49-3461-46-2879/2876; fax: +49-3461-46-2878.
E-mail address: martin.sommerfeld@iw.uni-halle.de (M. Sommerfeld).

0301-9322/03/$ - see front matter © 2003 Published by Elsevier Science Ltd.
doi:10.1016/S0301-9322(03)00031-4

1. Introduction

A channel or pipe flow is one of the simplest and best understood flow configuration in the area of single-phase flow and numerous experimental, theoretical and numerical investigations are available. If however particles are transported in such a flow system, the problem becomes considerably more difficult. Restricting our consideration to gas–particle flows only, one may have different flow regimes depending on conveying velocity and solids loading. Dilute phase pneumatic conveying of particles in pipes or channels is one of the most important technological process in industry and hence a huge amount of publications is available in this area, ranging from applied to very basic research. The reason for such numerous experimental studies is related to the complexity of a particle–laden flow in pipes or channels even in the dilute regime. The most important phenomena are:

- particle transport due to turbulence,
- strong shear flows and the resulting importance of the slip-shear lift force (Mei, 1992; Wang et al., 1997),
- Magnus effect since the particles acquire very high angular velocities when they collide with the walls (e.g. Matsumoto and Saito, 1970; Sommerfeld, 1996; Lun and Liu, 1997),
- wall collision effects may dominate the particle motion and affect the conveying characteristics (Adam, 1960; Brauer, 1980),
- wall roughness (Adam, 1960; Tsuji et al., 1987; Sommerfeld, 1992; Frank et al., 1993; Sommerfeld and Huber, 1999) and particle shape (Tsuji et al., 1991) will considerably affect the wall collision process,
- as a result of segregation effects (e.g. gravitational settling or particle inertia in bends or junctions) inter-particle collisions become already important at rather low mass loading (Burmester De Bessa Ribas et al., 1980; Oesterlé and Petitjean, 1993; Sommerfeld, 1995) and also the concentration distribution in vertical pipes is affected by inter-particle collisions (Sinclair and Jackson, 1989; Louge et al., 1991),
- as a function of particle size and mass loading the modulation of the flow and especially turbulence is an important issue (Gore and Crowe, 1989; Varaksin et al., 1998).

Numerous experimental and theoretical/numerical studies on the particle behaviour have been performed in the past and it is hardly possible to cover all this work in this article. Therefore, the most important studies of particle–laden gas flows in pipes or channels are summarised in Table 1 for the more experimental oriented examinations, and in Table 2 for those mainly concerned with modelling, numerical analysis and validation. In most of the experimental studies, the modulation of flow and turbulence by the particles was the main focus of research. Some of the early studies are those of Tsuji et al. (1982 and 1984) and Lee and Durst (1982) considering horizontal and vertical pipes and measuring air and particle velocity profiles by Laser–Doppler anemometers (LDA) with special discrimination procedures. A similar investigation was performed by Varaksin et al. (1998, 1999) for different particles transported in a vertical pipe. The studies mentioned in Lourenco et al. (1983) were performed in a horizontal channel flow and focussed on the modification of the gas velocity profiles by the particle phase which is in this configuration of course affected by gravitational settling. In all these studies wall roughness was not considered although it is an essential phenomenon.

Table 1
Summary of experimental studies on gas–particle channel and pipe flows

Reference	Flow configuration	Dimension	Gas velocity [m/s]	Type of particles	Particle density [kg/m^3]	Particle diameter [mm]	Mass loading [kg/kg]	Instrumentation
Matsumoto and Saito (1970)	Horizontal channel	$L = 6$ m, $H = 25$ mm	7 and 10	Polystyrene Glass Copper	1040 2500 8700	0.94 0.5 and 0.95 0.51	0.5	Visualisation
Lee and Durst (1982)	Vertical pipe	$L = D = 41.6$ mm	5.7	Glass beads	2500	0.1, 0.2, 0.4, and 0.8 mm	Up to 1.0	LDA
Lourenco et al. (1983)	Horizontal channel	$L =$ unknown 60×30 mm^2	6–13	Glass beads	2400	0.25 and 0.5	Up to 3.0	LDA
Tsuji et al. (1985)	Horizontal pipe	$L = 3.56$ m, $H = 30.5$ mm	7–20	Polystyrene	1000	0.2 and 3.4	Up to 5.0	LDA
Tsuji et al. (1984)	Vertical pipe	$L = 5.11$ m, $H = 30.5$ mm	8–20	Polystyrene	1000	0.243, 0.5, 1.42, and 2.8	Up to 5.0	LDA
Sommerfeld (1992)	Vertical channel	$H = 25$ mm	8.6	Glass beads	2500	0.45 and 0.11	Very low	LDA
Kulick et al. (1994)	Downward channel	$L = 5.0$ m, $H = 40$ mm	10.5	Lycopodium Glass beads Copper	300 2500 8700	0.1 and 0.5	Up to 0.8	LDA LDA
Huber and Sommerfeld (1994)	Different pipe elements	Different length $D = 80$ mm	10–30	Glass beads	2500	0.042 and 0.110	Up to 2.0	PDA, Imaging for concentration
Varaksin et al. (1998, 1999)	Vertical pipe	$L = 1.38$ m, $D = 46$ mm	5.2 and 6.4	Glass beads Aluminia	2550 3950	0.05 and 0.1 0.05	Up to 1.2	LDA
Sommerfeld and Huber (1999)	Horizontal channel	$L = 3.0$ m, $H = 30$ mm	5–15	Glass beads Quartz	2500 2400	0.1 and 0.5 0.2	Very low	Particle tracking (streak technique)
Kussin and Sommerfeld (2002)	Horizontal channel	$L = 6$ m, $H = 35$ mm	10–25	Glass beads Quartz	2500	0.06–1.0	Up to 2.0	PDA PIV

Table 2
Summary of numerical studies on gas–particle channel and pipe flows

Reference	Numerical method	Flow configuration, dimensions	Gas velocity [m/s]	Type of particles	Particle density [kg/m^3]	Lift forces	Wall collision	Inter-particle collision model
Ottjes (1978)	Predefined flow, particle tracking, no coupling	Horizontal pipe (two-dimensional) $D = 12$ mm	20	Spherical particles, 3 mm	820	Slip rotation	Inelastic, rotation, no roughness	No collisions
Tsuji and Morikawa (1978)	Predefined flow, particle tracking no coupling	Pipe bend ($D = 27$ and 50 mm)	10–20	Polystyrene 1.6 and 2.7 mm	1000	Slip rotation	Inelastic, rotation, no roughness	No collisions
Tsuji et al. (1987)	Euler/Lagrange, two-way coupling, no turbulence	Horizontal channel ($H = 25$ mm)	7 and 15	Polystyrene 1.0 mm	1000	Slip shear, slip rotation	Inelastic, rotation, virtual wall	No collisions
Tanaka and Tsuji (1991)	Predefined flow, particle tracking, no coupling	Vertical pipe, periodic domain ($D = 40$ mm)	16	Polystyrene 0.4 and 1.5 mm	1040	Slip shear, slip rotation	Inelastic, nonsphericalparticles	Deterministic, rotation
Tsuji et al. (1991)	Euler/Lagrange, two-way coupling, no turbulence	Horizontal pipe ($D = 52$ mm)	10	0.41–1.0 mm	1038	Slip shear, slip rotation	Inelastic, nonspherical particles	No collisions
Oesterlé (1991)	Predefined flow, particle tracking, no coupling	Pipe bend ($D = 80$ mm)	20 and 40	Spherical particles, 0.05 and 0.1 mm	2620	Slip shear, slip rotation	Inelastic	Stochastic, uncorrelated velocities
Sommerfeld and Zivkovic (1992)	Euler/Lagrange, two-way coupling	Horizontal channel ($H = 26$ mm) and pipe ($D = 80$ mm)	10.7 and 15	Glass beads 0.1 and 0.04 mm	2500	Slip shear, slip rotation	Inelastic, rotation, roughness	Stochastic, uncorrelated velocities
Oesterlé and Petitjean (1993)	Euler/Lagrange, no coupling	Horizontal pipe ($D = 30$ mm)	25.5	Spherical particles 0.1 mm	2620	Slip shear, slip rotation	Inelastic, rotation	Stochastic, uncorrelated velocities
Sommerfeld (1995)	Euler/Lagrange, no coupling	Horizontal channel ($H = 30$ mm)	20	Glass beads 0.045 and 0.1 mm	2500	Slip shear, slip rotation	Inelastic, rotation,wall roughness	Stochastic, uncorrelated velocities
Cao and Ahmadi (1995)	Euler/Euler, two-way coupling	Vertical pipe ($D = 30.5$ mm)	10–20	Polystyrene 0.2 and 0.5 mm	1040	Neglected	Slip boundary condition	Collisional stresses
Tu and Fletcher (1995)	Euler/Euler, no coupling	Channel bend	52	Spherical particles, 0.05 mm	2990	Neglected	No slip, generalised Eulerian	No collisions
Lun and Liu (1997)	Euler/Lagrange two-way coupling	Horizontal channel ($H = 25$ and 30 mm)	7–15	Glass beads 0.25 and 1.0 mm	2500	Slip shear, slip rotation	Inelastic, rotation	Deterministic
Huber and Sommerfeld (1998)	Euler/Lagrange four-way coupling	Horizontal pipe, pipe bend, vertical pipe ($D = 80$ and 150 mm)	24 and 27	Glass beads 0.04 mm	2500	Slip shear, slip rotation	Inelastic, rotation, wall roughness	Stochastic, uncorrelated velocities

One of the first theoretical and numerical studies on the effect of wall roughness or particle shape on the transport of particles in pipe or channel flows was performed by Matsumoto and Saito (1970), followed by a more detailed and extensive analysis in the research group of Tsuji (Tsuji et al., 1987, 1991; Tanaka and Tsuji, 1991). Here the virtual wall concept was introduced to avoid gravitational settling in glass pipes in order to match measured particle concentration profiles with those of numerical calculations. Physically, this approach however may not be regarded as a wall roughness model, since spherical glass beads and a smooth glass pipe were considered in the experiments and the virtual wall was introduced conditionally when the impact angle became lower than a certain value. Thereafter, it was demonstrated that also slight non-spherical glass beads or polystyrene particles might be responsible for avoiding gravitational settling due to redispersion effects. In the paper of Tsuji et al. (1989) a detailed wall collision model for non-spherical particles was introduced.

A physically founded wall roughness model was first introduced by Sommerfeld (1992), who demonstrated the strong effect of wall roughness on the particle fluctuating motion in a vertical channel flow. This model was further refined and improved based on detailed measurements by applying particle steak line velocimetry in a particle–laden horizontal channel flow (Sommerfeld and Huber, 1999). Numerical calculations of particle transport in different pipe elements consisting of stainless steel or glass with appropriate wall roughness modelling were conducted by Huber and Sommerfeld (1998). By comparison of the computations for smooth and rough walls in a horizontal pipe, the dispersion effect of wall roughness has been clearly confirmed. The comparison of the calculation with the experiments (see also Huber and Sommerfeld, 1994) has shown very good agreement for the horizontal pipe demonstrating the appropriate modelling of wall roughness.

Inter-particle collisions can be described by deterministic as well as stochastic models. In dilute phase pneumatic conveying a deterministic collision model was applied by Tanaka and Tsuji (1991) in the frame of a Lagrangian method. In order to restrict the computational effort, only a short vertical pipe element was considered by using periodic boundary conditions and tracking only 1000 particles simultaneously. Turbulence effects could be neglected, since the particles were rather large. However, an interesting effect was reported, namely that the components of the particle fluctuation velocities became more isotropic due to inter-particle collisions caused by the redistribution of the particle momentum from the main stream to the transverse direction.

A stochastic approach for inter-particle collisions is for example the Monte-Carlo method introduced by Ogawa (1983) or the so-called direct simulation Monte-Carlo (DSMC) method introduced by Tsuji (1993), which are both based on procedures to simulate the Boltzmann equation. Inter-particle collisions in dilute phase pneumatic conveying by applying a stochastic model in the frame of the Euler/Lagrange approach were considered in the work of Sommerfeld and Zivkovic (1992) and Oesterlé and Petitjean (1993). Such a stochastic collision model is computationally very efficient and does not require information on the location and motion of neighbouring particles in order to decide whether a collision occurs. Instead, a fictitious collision partner is generated which is a representative of the local particle phase properties and the occurrence of a collision is decided based on the collision probability according to kinetic theory of gases. In both papers, the enormous importance of inter-particle collisions even at low overall mass loading for the development of the particle concentration profiles in a horizontal channel has been emphasised. This is caused by the redistribution of the particle momentum from the

streamwise to the lateral component by inter-particle collisions and results in an enhancement of the lateral dispersion whereby gravitational settling is reduced (Burmester De Bessa Ribas et al., 1980; Tsuji et al., 1987; Sommerfeld, 1995). Moreover, numerical calculations with inter-particle collisions were performed by Louge et al. (1991) and Cao and Ahmadi (1995) using a two-fluid formulation and Lun and Liu (1997) by applying a deterministic collision model in the frame of the Euler/Lagrange approach.

In the present study the importance of wall collisions including the effect of wall roughness and inter-particle collisions for the particle motion in a horizontal channel flow is analysed thoroughly on the basis of numerical calculations using the Lagrangian approach. In comparison to previous work (Sommerfeld, 1995, 1998), the effect of wall roughness is considered. Moreover, the wall collision mean free path is introduced to characterise the particle behaviour for calculations with different model assumptions. Such a separation of the physical effects influencing the particle motion is experimentally impossible and the introduced numerical calculations allow a much better insight into the particle transport phenomena in horizontal pneumatic conveying.

2. Numerical approach

In the present study two-dimensional numerical calculations are performed, in order to analyse the particle behaviour and to evaluate the effects of wall collisions, wall roughness and inter-particle collisions in a horizontal channel flow. Moreover, integral parameters to characterise the particle phase behaviour are derived. The considered approach is based on prescribing the gas flow field. Hence, two-way coupling effects are not considered in this study, which is a valid assumption for the considered inertial particles. This implies that constant profiles of the mean velocities and mean fluctuating components for the gas phase are given along the channel. For the gas velocity profile a potential law with an exponent of 1/7 was used. The rms-values of the fluid velocity fluctuations in the streamwise and lateral directions were taken from the measurements of Laufer (1950) by accounting for the considered average gas velocity. The agreement of the flow field with the performed single-phase experiments was found to be reasonably good (Kussin and Sommerfeld, 2002). In order to determine the profiles of the turbulent time and length scales the dissipation rate ε was calculated in the standard way:

$$\varepsilon = C_\mu^{0.75}\frac{k^{1.5}}{l_\mathrm{m}} \quad \text{with } C_\mu = 0.09, \;\; l_\mathrm{m} = h\left(0.14 - 0.08\left(1-\frac{y}{h}\right)^2 - 0.06\left(1-\frac{y}{h}\right)^4\right)$$

where k is the turbulent kinetic energy, l_m the mixing length for a channel (Schlichting, 1982), h the channel half width and y the transverse co-ordinate measured from the wall of the channel. In connection with the Langevin dispersion model which will be described briefly below, the integral time scale and length scales in the streamwise and lateral directions (i.e. y and z) were determined from

$$T_\mathrm{L} = 0.16\frac{k}{\varepsilon}, \quad L_x = 2.45 T_\mathrm{L}\sqrt{k}, \quad L_{y,z} = 0.5 L_x$$

The Lagrangian approach is used to simulate the particle phase based on recent developments to model the relevant physical effects which describes the particle motion, wall collisions, wall

roughness, and inter-particle collisions. A sufficiently large number of particles were tracked through the flow field to obtain ensemble averaged properties for the particle phase at the end of the channel. In applying this approach two-way coupling effects are neglected in order to allow solely the analysis of wall collision and inter-particle collision effects as a function of loading ratio and particle size without having modulations of the flow field by the particles. Each parcel represents a number of real particles with the same properties in order to ensure the representation of the dispersed phase concentration by a reasonable number of computational particles. The parcels are tracked through the flow field by solving the equations of motion, a set of ordinary differential equations for the calculation of the new parcel position, the parcel linear velocity components, and the angular velocity. The forces considered to act on the particle are the drag force, the gravity, the slip-shear lift force, and the lift force resulting from particle rotation. This yields the following set of equations for the calculation of the particle motion:

$$\begin{aligned} \frac{\mathrm{d}\vec{x}_\mathrm{p}}{\mathrm{d}t} &= \vec{u}_\mathrm{p} \\ m_\mathrm{p}\frac{\mathrm{d}\vec{u}_\mathrm{p}}{\mathrm{d}t} &= \vec{F}_\mathrm{D} + \vec{F}_\mathrm{g} + \vec{F}_\mathrm{LS} + \vec{F}_\mathrm{LR} \\ I_\mathrm{p}\frac{\mathrm{d}\vec{\omega}_\mathrm{p}}{\mathrm{d}t} &= \vec{T} \end{aligned} \tag{1}$$

Here, $\vec{x}_\mathrm{p}$ is the particle position vector, $\vec{u}_\mathrm{p}$ is the particles translational velocity vector, $\vec{\omega}_\mathrm{p}$ is the angular velocity vector, m_p is the particle mass, and I_p is the moment of inertia. The last equation (Eq. (1)) considers the change of particle rotation due to the viscous interaction with the surrounding fluid. The considered forces and the torque acting on the particle are introduced in the following for completeness (see also Sommerfeld, 2000). The drag force is calculated from

$$\vec{F}_\mathrm{D} = \frac{3}{4}\frac{\rho_\mathrm{f} m_\mathrm{p}}{\rho_\mathrm{p} D_\mathrm{p}} c_\mathrm{D}(\vec{u}_\mathrm{f} - \vec{u}_\mathrm{p})|\vec{u}_\mathrm{f} - \vec{u}_\mathrm{p}| \tag{2}$$

where the drag coefficient c_D is obtained from the correlations:

$$\begin{aligned} &c_\mathrm{D} = \tfrac{24}{Re_\mathrm{p}}(1 + 0.15Re_\mathrm{p}^{0.687}) = \tfrac{24}{Re_\mathrm{p}} f_\mathrm{D}, \quad && Re_\mathrm{p} \leqslant 1000 \quad && Re_\mathrm{p} = \frac{\rho_\mathrm{f} D_\mathrm{p}^2 |\vec{u}_\mathrm{f} - \vec{u}_\mathrm{p}|}{\mu_\mathrm{f}} \\ &c_\mathrm{D} = 0.44, && Re_\mathrm{p} > 1000 \end{aligned} \tag{3}$$

The slip-shear lift force is based on the analytical result of Saffman (1965) which was extended for higher particle Reynolds numbers (Mei, 1992; Crowe et al., 1998):

$$\vec{F}_\mathrm{LS} = 1.615 D_\mathrm{p}^2 (\rho_\mathrm{f}\mu_\mathrm{f})^{1/2} \left(\frac{1}{|\vec{\omega}_\mathrm{f}|}\right)^{0.5} \{(\vec{u}_\mathrm{f} - \vec{u}_\mathrm{p}) \times \vec{\omega}_\mathrm{f}\} f(Re_\mathrm{p}, Re_\mathrm{s}) \tag{4}$$

where the fluid rotation is given by

$$\vec{\omega}_\mathrm{f} = 0.5\nabla \times \vec{u}_\mathrm{f} \tag{5}$$

and the ratio of extended lift force to the Saffman force is

$$f(Re_\mathrm{p}, Re_\mathrm{s}) = \frac{F_\mathrm{LS}}{F_\mathrm{LS,Saff}}$$

$$\begin{aligned} \frac{F_{\mathrm{LS}}}{F_{\mathrm{LS,Saff}}} &= (1-0.3314\beta^{1/2})\exp\left(-\tfrac{Re_{\mathrm{p}}}{10}\right)+0.3314\beta^{1/2} \quad \text{for } Re_{\mathrm{p}} \leqslant 40 \\ &= 0.0524(\beta Re_{\mathrm{p}})^{1/2} \quad \text{for } Re_{\mathrm{p}} \geqslant 40 \end{aligned} \tag{6}$$

The parameter β is given by

$$\beta = \frac{1}{2}\frac{Re_{\mathrm{s}}}{Re_{\mathrm{p}}} \tag{7}$$

where Re_{s} is the Reynolds number of the shear flow:

$$Re_{\mathrm{s}} = \frac{\rho_{\mathrm{f}} D_{\mathrm{p}}^2 |\vec{\omega}_{\mathrm{f}}|}{\mu_{\mathrm{f}}} \tag{8}$$

The rotational lift force and the torque (Eq. (1)) for a rotating sphere moving in a stagnant fluid were derived by Rubinow and Keller (1961). These relations were extended to include the relative motion between particle and moving fluid in the following way (Crowe et al., 1998):

$$\vec{F}_{\mathrm{LR}} = \frac{\rho_{\mathrm{f}}}{2}\frac{\pi}{4} D_{\mathrm{p}}^2 C_{\mathrm{LR}} |\vec{u}_{\mathrm{f}} - \vec{u}_{\mathrm{p}}| \frac{\vec{\Omega} \times (\vec{u}_{\mathrm{f}} - \vec{u}_{\mathrm{p}})}{|\vec{\Omega}|} \tag{9}$$

where $\vec{\Omega}$ represents the relative rotation, i.e. $\vec{\Omega} = \vec{\omega}_{\mathrm{f}} - \vec{\omega}_{\mathrm{p}}$. For small particle Reynolds numbers the lift coefficient is obtained according to Rubinow and Keller (1961) in the form:

$$C_{\mathrm{LR}} = \frac{D_{\mathrm{p}}|\vec{\Omega}|}{|\vec{u}_{\mathrm{f}} - \vec{u}_{\mathrm{p}}|} = \frac{Re_{\mathrm{R}}}{Re_{\mathrm{p}}} \tag{10}$$

with

$$Re_{\mathrm{R}} = \frac{\rho_{\mathrm{f}} D_{\mathrm{p}}^2 |\vec{\Omega}|}{\mu_{\mathrm{f}}} \tag{11}$$

being the Reynolds number of particle rotation. A lift coefficient for higher particle Reynolds numbers requires experimental information. Recently, Oesterlé and Bui Dinh (1998) introduced the following correlation based on available literature data and additional experiments for $Re_{\mathrm{p}} < 140$:

$$C_{\mathrm{LR}} = 0.45 + \left(\frac{Re_{\mathrm{R}}}{Re_{\mathrm{p}}} - 0.45\right)\exp(-0.05684 \cdot Re_{\mathrm{R}}^{0.4} \cdot Re_{\mathrm{p}}^{0.3}) \quad \text{for } Re_{\mathrm{p}} < 140 \tag{12}$$

The torque acting on a rotating particle due to the viscous interaction with the fluid was also derived by Rubinow and Keller (1961) for a stagnant fluid and small particle Reynolds numbers. This expression may be extended for a three-dimensional flow and for higher Reynolds numbers by introducing a rotational coefficient:

$$\vec{T} = \frac{\rho_{\mathrm{f}}}{2}\left(\frac{D_{\mathrm{p}}}{2}\right)^5 C_{\mathrm{R}} |\vec{\Omega}| \vec{\Omega} \tag{13}$$

From the numerical simulations of Dennis et al. (1980) and experimental data of Sawatzki (1970) the rotational coefficient for higher particle Reynolds numbers is found to be

$$C_R = \frac{12.9}{Re_R^{0.5}} + \frac{128.4}{Re_R} \quad \text{for } 32 < Re_R < 1000 \tag{14}$$

In the case of smaller particle Reynolds numbers the result of Rubinow and Keller (1961) yields

$$C_R = \frac{64\pi}{Re_R} \quad \text{for } Re_R < 32 \tag{15}$$

The lift forces are of importance in strong shear gradients and for rotating particles. Particle rotation is mainly induced by wall collisions. The importance of the lift forces has been analysed in detail through numerical computations by Sommerfeld (1996).

The above equations for the particles are integrated by an analytical approach (Huber and Sommerfeld, 1998). Since the most dominant force is the drag force, all other forces may be considered to be constant during the time interval of the integration (i.e. the Lagrangian time step Δt) if this is sufficiently small. The time step is chosen to be 20% of the minimum of all the local relevant time scales (i.e. associated with the control volume where the particle is located), such as

Particle relaxation time:

$$\tau_p = \frac{\rho_p D_p^2}{18\mu_f f_D} \tag{16}$$

Time scale of turbulence:

$$T_L = 0.16\frac{k}{\varepsilon} \tag{17}$$

Inter-particle collision time:

$$\tau_C = \frac{1}{\frac{\pi}{4}(D_{pl} + D_{pu})^2 \Delta U_{pmax} N_p} \tag{18}$$

The local average particle relaxation time according to Eq. (16) is obtained from the calculations. The integral time scale of turbulence is specified according to the Langevin model used to describe particle dispersion (see Sommerfeld et al., 1993). For the calculation of the inter-particle collision time the sum of the considered minimum and maximum particle diameter is selected and the relative velocity is estimated from the maximum relative velocity between the particles. The particle number concentration N_p is defined as particles/m^3.

The instantaneous fluid velocity components at the particle location, which have to be known for solving the equations of motion (Eq. (1)), were determined from the local mean fluid velocity interpolated from the neighbouring grid points and a fluctuating component generated by the Langevin model described by Sommerfeld et al. (1993). In this model the fluctuating velocity components are composed of a correlated part from the previous particle location and time step, and a random component sampled from a Gaussian distribution function. The correlation function is composed of a Lagrangian and an Eulerian part to account for the crossing trajectories effect and is calculated using appropriate time and length scales given above. This model was thoroughly validated for a number of test cases, such as grid turbulence and pipe flows (Sommerfeld et al., 1993).

The wall collision of particles is particularly important in wall bounded flows, such as channel or pipe flows. The change of the particles linear and angular velocities was calculated by solving the impulse equations in connection with Coulomb's law of friction in order to yield two sets of equations for a sliding and non-sliding bouncing process (Tsuji et al., 1987; Huber and Sommerfeld, 1998). Additionally, the model accounts for the particle rotation. Since wall roughness is very important and may considerably alter the particle motion, a model has been developed which relies on detailed experiments (Sommerfeld and Huber, 1999). The model is based on the assumption, that the particle impact angle is composed of the particle trajectory angle and a random normal distributed component due to roughness. The standard deviation of the so-called roughness angle of course is depending on the roughness height distribution and the particle size. From the measurements the dependence of the standard deviation of the roughness angle distribution from the particle size has been derived. Moreover, the so-called shadow effect was accounted for, which implies that the probability of particles hitting a negative roughness structure at shallow impact angles is reduced. This results in an average rebound angle which is slightly larger than the particle impact angle, causing however a strong enhancement of the wall-normal velocity component and a redispersion of particles in a horizontal channel (Sommerfeld, 1995). In addition to the standard deviation of the roughness, the restitution coefficient and the friction coefficient were obtained from the experiments. The model applied for the present analysis was validated thoroughly by Sommerfeld and Huber (1999). In the wall collision model a linear variation of the restitution ratio from 1.0 to 0.7 up to an impact angle of 25° (measured from the wall) and a constant value of 0.7 for larger impact angles was used. A similar correlation was applied for the dependence of the friction coefficient on the impact angle, namely a decrease form 0.5 at zero impact angle to 0.15 at an impact angle of 25° and a constant value of 0.15 for larger impact angles.

The standard deviation of the roughness angle was only measured for the 100 and 500 μm glass beads (Sommerfeld and Huber, 1999). Therefore, the correlation specified in Fig. 1 was elaborated in order to allow the proper consideration of the roughness angle as a function of particle size. In addition some calculations were also performed with a lower degree of roughness, which is also indicated in Fig. 1. These two degrees of roughness correspond to recent measurements performed

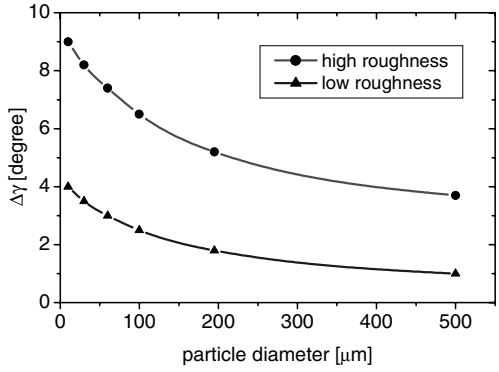

Fig. 1. Standard deviation of the wall roughness angle distribution as a function of particle diameter.

by Kussin and Sommerfeld (2002). The correlations for both degrees of roughness are given as follows (HR: high roughness, LR: low roughness):

$$\Delta\gamma_{\mathrm{HR}} = 3.4963 + 5.797 \cdot \exp\left(-\frac{D_{\mathrm{p}}}{154.12}\right)$$

$$\Delta\gamma_{\mathrm{LR}} = 1.551 + 3.438 \cdot \exp\left(-\frac{D_{\mathrm{p}}}{161.55}\right)$$

In the present paper however results are presented for a smooth channel and the high roughness case.

Inter-particle collisions were described by the stochastic collision model developed and validated by Sommerfeld (2001). This model is based on the generation of a fictitious collision partner during each time step of tracking the considered particle (i.e. parcel). The properties of the fictitious particle, i.e. size and velocities, are sampled from local distribution functions by accounting however, for a possible correlation of the velocity fluctuation of the fictitious particle. This correlation depends on particle inertia (i.e. particle Stokes number) and gives the correct values for very heavy particles (i.e. kinetic theory limit) and for light particles (i.e. turbulent shear limit). Especially, for small Stokes numbers the effect of the correlated motion of particles in turbulence can drastically reduce collision frequency. The occurrence of collisions is decided by calculating the collision probability from kinetic theory and using a random process to generate the point of impact (Sommerfeld, 2001). It should be noted however, that this model assumes a collision efficiency of 100% and hence is not appropriate for particles of large size difference. However, the present study is based on the consideration of mono-sized particles. The post collision properties, i.e. linear and angular velocities, of the considered particle are obtained by solving the impulse equations in connection with Couloumb's law of friction. This results in two sets of equations for a sliding and a non-sliding collision. This model also includes the effect of particle rotation. The restitution ratio was assumed to be 0.9 and a constant value of 0.4 was used for the friction coefficient.

3. Interpretation of particle motion in channel flows

In the following section the effect of wall collisions and wall roughness on the behaviour of spherical particles with different size and a density of $\rho_{\mathrm{p}} = 2.5$ g/cm^3 in a horizontal channel of 35 mm height and a length of 6 m is analysed. The gas flow field (i.e. mean velocity and turbulence) was prescribed according to the measurements of Laufer (1950) for a fully developed channel flow with an average velocity of 18 m/s and two-way coupling was neglected, as mentioned above. The gas density was given a value of 1.18 kg/m^3 and the dynamic viscosity was selected to be 18.8×10^{-6} N s/m^2. In order to get statistical reliable data typically about 20,000 parcels are tracked sequentially through the flow field. This approach is justified, since only the steady state result is of interest. In all the calculations mono-sized particles in the size range between 30 and 700 μm are considered. The averaged particle response times and an estimate of the particle Stokes numbers calculated with the integral time scale of turbulence on the centre-line are

provided in Table 3. The Stokes number indicates that only the motion of the 30 and 60 μm particles will be affected by turbulence.

In Fig. 2 the behaviour of spherical glass beads with different diameter in a channel without and with wall roughness is illustrated. Please note that the height to length ratio of the channel has been considerably changed in the graphs for clarity, i.e. the channel length is 6 m and the height is 35 mm. First of all the results demonstrate that small particle (i.e. 30 μm) are slightly affected by

Table 3
Characterisation of particles used for the numerical calculations

Particle diameter [μm]	Averaged particle response time [ms]	Stokes number
30	5.4	1.4
60	17.6	4.6
110	42.6	11.2
195	93.0	24.3
300	158.0	41.4
500	288.6	75.5
700	417.2	109.2

The particle response time is an average of all particles tracked through the channel and accounts for non-linear drag ($U_{av} = 18$ m/s, $\eta = 1.0$, with wall roughness and inter-particle collisions); the Stokes number is defined as $St = \tau_p/T_L$, where the integral time scale on the centre-line of the channel is used $T_L = 3.8$ ms.

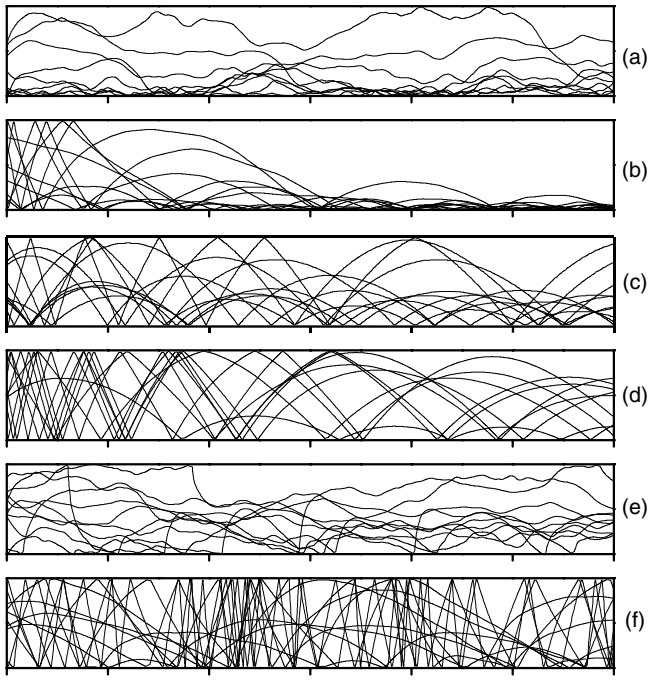

Fig. 2. Calculated particle trajectories in a horizontal channel flow (channel height 35 mm and length 6 m, length and height of the graphs correspond to these dimensions), without wall roughness: (a) 30 μm, (b) 110 μm, (c) 195 μm, (d) 300 μm, with wall roughness: (e) 30 μm, (f) 110 μm ($U_{av} = 18$ m/s, $\eta = 0.1$).

turbulence, whereas the motion of larger particles is governed by inertia. Moreover, it is obvious that the wall roughness has a strong effect on the particle motion, especially for larger particles (compare Fig. 2c and f), whereby they bounce from wall to wall. Please note, that the horizontal distance between subsequent wall collisions is still about 0.5 m in the case of roughness (Fig. 2f). Also the small particles are better dispersed by accounting for the wall roughness effects (compare Fig. 2a and e). The result of the particle trajectory calculation may be summarised by plotting the wall collision mean free path over the particle response time (Fig. 4). The particle response time was determined from the calculations by averaging all particles and accounting for the non-linear drag (Eq. (3)). The wall collision mean free path is defined to be the average horizontal distance between subsequent wall collisions with the lower and upper wall of the channel, averaged over the last 2 m of the channel for all the parcels.

Considering the results without wall roughness and inter-particle collisions (Fig. 4), it is obvious that small particles are considerably dispersed by turbulence (see also Fig. 2a), whereby the wall collision frequency is relatively low (i.e. the wall collision mean free path is large). Increasing particle size results in a decrease of the wall collision mean free path and a minimum is obtained for the present flow condition and channel height for a particle response time of about 30 ms, which corresponds to particles with a size of about 80 μm in case $\rho_p = 2.5$ g/cm^3. In this region the particles bounce along the lower wall after some distance of development downstream from the inlet. This reveals that these heavier particles are strongly affected by gravity, implying that they perform a saltating motion without contacting the upper wall (see also Fig. 2b). A further increase in particle size again results in a bouncing from wall to wall due to the increasing particle inertia (Fig. 2c) and the wall collision mean free path approaches a maximum (i.e. the wall collision frequency reaches a minimum). For even larger particles a slightly reduction of wall collision mean free path is observed, caused by the bouncing of the particles from wall to wall (Fig. 2d). By neglecting the lift forces (i.e. slip-shear and slip-rotation) in the particle tracking, the wall collision mean free path is decreased for the entire particle size range due to the missing action of the lift forces towards the centre of the channel (Fig. 4). Of course all other calculations were performed with the lift forces.

In case a channel without any wall roughness is considered for conveying the particles, the effect of inter-particle collisions becomes very important even at moderate mass loading (Sommerfeld, 1998). The main effect of inter-particle collisions is observed in the regime of saltating particle motion, in this case below $\tau_p \approx 150$ ms, corresponding to a particle size of about 250 μm (Figs. 3 and 4). In this region, the particles become considerably better dispersed with increasing loading since the particle collision frequency is increasing, resulting in a drastic increase of wall collision mean free path (Fig. 4). The trajectories of 110 μm particles in Fig. 3b show very clearly that in a smooth channel inter-particle collisions result in a pronounced dispersion of the particles. With increasing particle response time beyond 150 ms a slight reduction of the mean free path is observed and the values are almost identical with those obtained without inter-particle collisions. It should be noted at this point, that calculations are compared for constant mass loading so that an increasing particle size also results in a reduction of the number density and thus inter-particle collision frequency.

By plotting the wall collision mean free path over the particle response time for the case of wall roughness the picture changes completely (Fig. 5). It becomes obvious, that for the regime of larger particles ($\tau_p > 50$ ms) the mean free path between wall collisions is considerably shorter

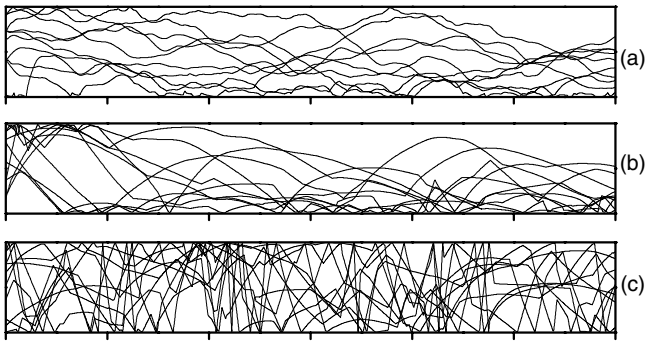

Fig. 3. Calculated particle trajectories in a horizontal channel flow by accounting for inter-particle collisions with $\eta = 1.0$ (channel height 35 mm and length 6 m, length and height of the graphs correspond to these dimensions), without wall roughness: (a) 30 μm, (b) 110 μm, with wall roughness: (c) 110 μm ($U_{av} = 18$ m/s).

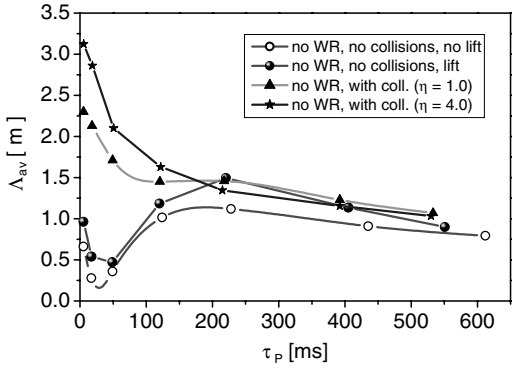

Fig. 4. Calculated wall collision mean free path as a function of particle response time by neglecting wall roughness for a horizontal channel of 35 mm height and 6 m length ($U_{av} = 18$ m/s).

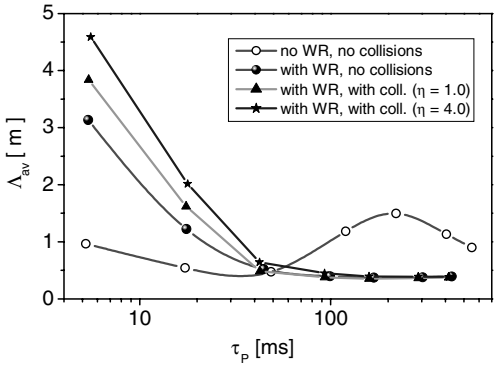

Fig. 5. Calculated wall collision mean free path as a function of particle response time, illustrating the effect of wall roughness (horizontal channel of 35 mm height and 6 m length, $U_{av} = 18$ m/s).

compared to the case with smooth wall. In this regime only a small variation of the mean free path with mass loading and consequently increasing inter-particle collision frequency is observed. Hence, the particle motion is almost completely controlled by wall collisions and wall roughness. For small particles, i.e. below a particle response time of about 40 ms, the mean free path between wall collisions is considerably higher than for the case without roughness if no collisions are considered and considerably increases with decreasing particle size. Moreover, increasing particle mass loading results in a remarkable increase of the mean free path as a result of inter-particle collisions. This of course implies a better dispersion of the particles (Fig. 5). The effect of inter-particle collisions on the particle concentration distribution in the channel is illustrated in Fig. 6 for 60 and 110 μm particles. For both cases a developed flow seems to be reached after a distance of 2–3 m. The smaller particles (i.e. 60 μm) exhibit a pronounced gravitational settling, although wall roughness is considered. Inter-particle collisions drastically reduce the particle concentration near the bottom of the channel and a maximum is formed in the core of the channel. Even in the case of 110 μm particles inter-particle collisions improve the dispersion (Fig. 6) although the wall collision mean free path does not change considerably. This is caused by the fact that without collisions the particles perform a saltating motion and bounce along the lower wall and with inter-particle collisions at higher loading they also will collide with the upper wall. A comparison with the result obtained without wall roughness reveals that for small particles roughness reduces the wall collision frequency, while for large particles an enhancement is found. Therefore, also the pressure loss should be differently affected for small and large particles, which yet has to be confirmed experimentally.

In order to allow a better illustration of the particle dispersion characteristics as a function of mass loading (i.e. effect of inter-particle collisions) and additionally with the effect of wall roughness, vertical profiles of the particle mass flux at the end of the channel normalised by the average flux are shown in Figs. 7 and 8 for different particle diameters. The particle size was selected to cover the lower range of particle relaxation times where the effects explained above are

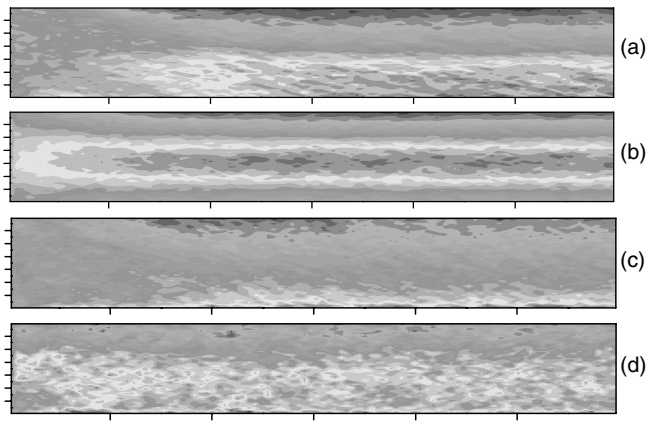

Fig. 6. Calculated distribution of particle concentration demonstrating the effect of inter-particle collisions (channel height 35 mm and length 6 m, length and height of the graphs correspond to these dimensions), $D_p = 60$ μm: (a) no collisions, (b) with collisions, $D_p = 110$ μm: (c) no collisions, (d) with collisions (with wall roughness, $U_{av} = 18$ m/s, $\eta = 1.0$).

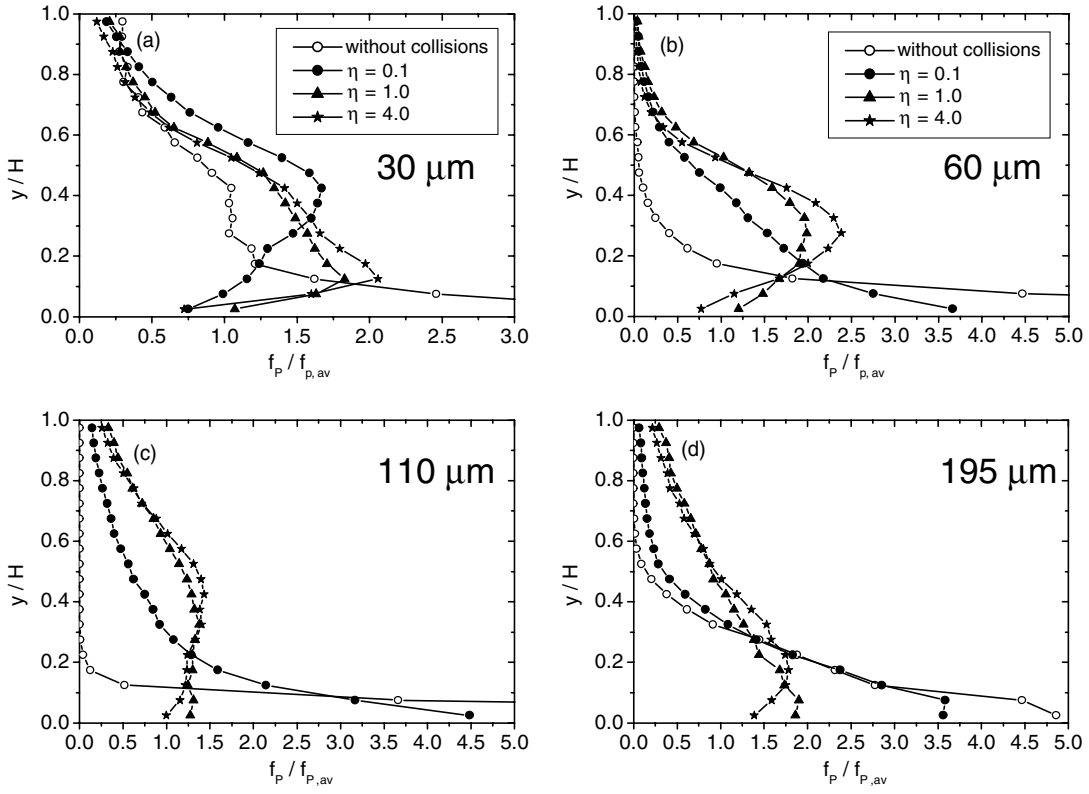

Fig. 7. Vertical profiles of the normalised particle mass flux in the horizontal direction for the case without wall roughness and different particle diameters, (a) $D_p = 30$ μm, (b) $D_p = 60$ μm, (c) $D_p = 110$ μm, (d) $D_p = 195$ μm ($H = 35$ mm, $U_{av} = 18$ m/s).

most pronounced (i.e. as demonstrated in Figs. 4 and 5). The mass flux profiles in Fig. 7 correspond to the case with the smooth wall and hence the dispersion effects observed are caused solely by inter-particle collisions. Without collisions, gravitational settling is observed for all particle sizes and high particle mass flux is found near the bottom of the channel. In case the particles are larger they are not sufficiently dispersed by turbulence and hence a particle-free region develops near the top region of the channel. Hence, a relatively dense rope is formed near the bottom. It should be mentioned that beyond the minimum of the wall collision mean free path (see Fig. 4) inertial effects dominate particle motion, whereby they bounce from wall to wall (see Fig. 2). By considering inter-particle collisions the particles become considerably better dispersed across the channel and the mass flux maximum near the bottom is reduced. Eventually, at high enough mass loading a new maximum develops at some distance above the channel bottom, depending on the particle inertia. This reveals that due to high collision rate the particles are flanged out of the dense region near the bottom by inter-particle collisions, which is caused by the fact that in the near-wall region high relative velocities between the particles develop, since particles are found which move towards the wall and those which are reflected from the wall. Near the bottom of the channel these effects also result in a maximum of the collision frequencies (Fig. 9). For the particle

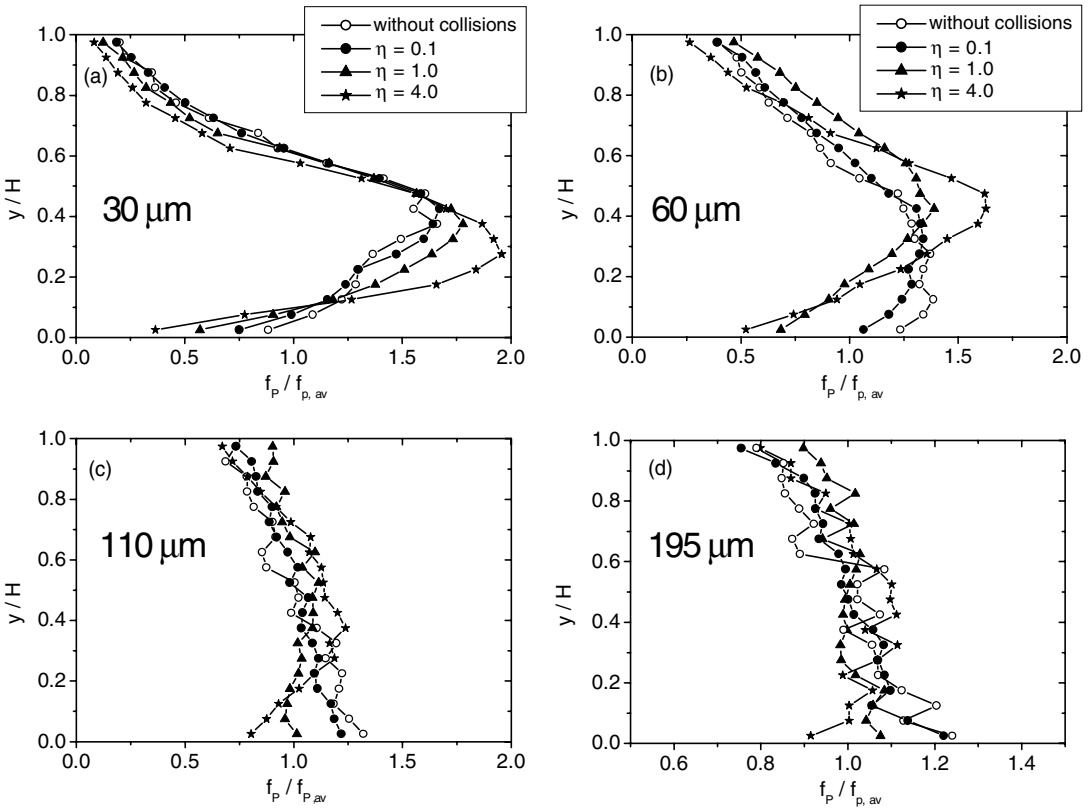

Fig. 8. Vertical profiles of the normalised particle mass flux in the horizontal direction for the case with wall roughness (HR) and different particle diameters, (a) $D_p = 30$ μm, (b) $D_p = 60$ μm, (c) $D_p = 110$ μm, (d) $D_p = 195$ μm ($H = 35$ mm, $U_{av} = 18$ m/s).

sizes analysed, the collision frequency considerably increases from the top to the bottom of the channel for the case of smooth walls.

For the smaller particles considered (for this configuration up to a particle size of 110 μm) a drastic modification of the mass flux profiles is already found for a mass loading of 0.1 when accounting for inter-particle collisions. This demonstrates that even at such low mass loading neglecting of inter-particle collisions gives completely erroneous results. Moreover, for the smallest particles (i.e. 30 μm), where turbulent transport is of importance, also inter-particle collisions have a pronounced and interesting effect. The consideration of inter-particle collisions at $\eta = 0.1$ causes a very good dispersion of the particles and the maximum of the flux is found 40% above the channel bottom. A further increase of mass loading and hence inter-particle collision frequency causes again a downward shift of the flux maximum. This implies that particles rebound from the bottom wall are not able to reach a higher elevation, since the probability of collisions with particles approaching the wall increases due to the increase in number density. However, the maximum in the collision frequency remains near the bottom due to high relative velocity (Fig. 9). For the other cases such high number densities are not reached since the

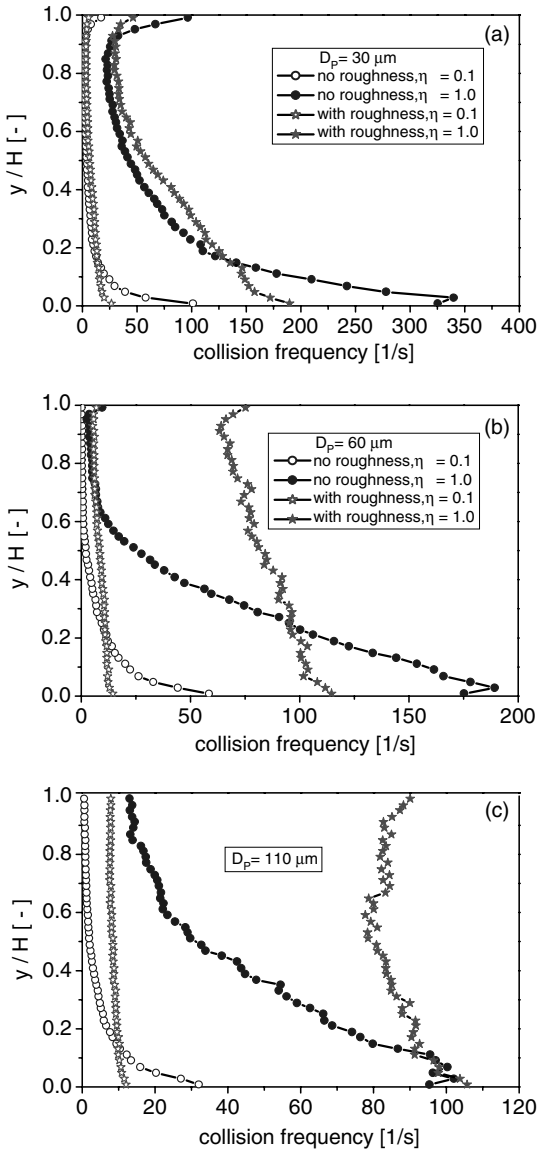

Fig. 9. Vertical profiles of particle collision frequency with and without wall roughness (HR) and different particle diameters, (a) $D_p = 30$ μm, (b) $D_p = 60$ μm, (c) $D_p = 110$ μm ($H = 35$ mm, $U_{av} = 18$ m/s).

comparison is done (as usual) for constant mass loading, which implies a decrease of particle number density with increasing particle diameter. But also here (i.e. in these studies 110 and 195 μm) gravitational settling is reduced and the maximum in the flux appears at some distance above the bottom for higher mass loading (Fig. 7). The profiles of the collision frequency for the smooth wall also show their maximum near the bottom and a drastic decrease towards the top of the channel (Fig. 9).

The particle mass flux profiles in Fig. 8 are obtained by accounting for the wall roughness effect (higher roughness specified in Fig. 1). This result reveals that already without inter-particle collisions (i.e. at very low particle mass loading) gravitational settling is avoided by the dispersion effect of wall roughness (Sommerfeld and Huber, 1999) for all particle sizes considered. Moreover, inter-particle collision effects are more pronounced for smaller particles (in this configuration for the 30 and 60 μm particles), where the turbulent transport plays a stronger role than for the larger particles which are dominated strongly by wall collisions and consequently are already very good dispersed without collisions. For such large particles inter-particle collisions cause only a slightly better dispersion and a slight reduction of the mass flux near the bottom is observed with increasing mass loading. However, collisions will have an effect on momentum transfer, and modify the fluctuating behaviour of the particles. The motion of particles larger than about 200 μm is completely governed by wall collision effects and only very small modifications of the flux profiles with increasing loading are observed (not shown here). Again it should be mentioned that the number concentration is decreasing with particle size if mass loading is kept constant.

Considering the profiles of the inter-particle collision frequency for the case with roughness, shows for smaller particles (i.e. 30 μm) still a notable increase from the top to the bottom of the channel (Fig. 9). However, for the larger particles the values of the collision frequency become more or less constant across the channel with a slight increase towards the bottom. In all cases a small increase of the collision frequency towards the walls is observed due to the random rebound of the particles. As one would expect from Fig. 9, the average values of the collision frequencies are considerably higher in the case of wall roughness except for the small particles which are more strongly transported by turbulence. The average collision frequency as a function of particle response time is summarised in Fig. 10 for a mass loading of one. Without roughness the collision frequency decreases exponentially due to the decreased particle number density at fixed mass loading. For the rough wall initially (i.e. up to $\tau_p = 50$ ms) the collision frequency increases due to the modification of particle dispersion behaviour (see Fig. 8). With further increase of particle size also an exponential decrease of the average collision frequency is found. The higher average

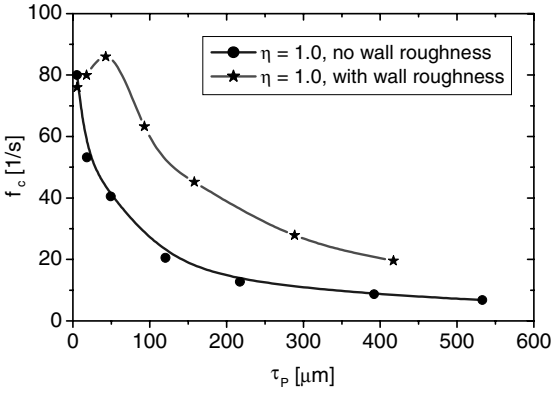

Fig. 10. Average collision frequency along the channel as a function of particle response time without and with wall roughness ($H = 35$ mm, $\eta = 1.0$, $U_{av} = 18$ m/s).

collision frequencies for the case with roughness are mainly associated with the higher particle velocity fluctuations.

The coupling between wall collision frequency and particle velocity is demonstrated in Fig. 11 for different particle sizes. This clearly shows that the particle transport velocity is considerably decreased by the enhancement of wall collisions due to roughness for the larger particles. For the small particles (i.e. 60 μm), the horizontal component of the particle velocity is decreased in the core of the channel and considerably increased near the walls as a result of wall roughness. Especially, near the lower wall this effect is pronounced. This is caused by the better lateral dispersion of the small particles which is also obvious from the increase of the lateral particle velocity fluctuation originating from the wall roughness. Moreover, Fig. 5 reveals an increase in the wall collision mean free path for smaller particles when wall roughness is accounted for. This should reduce the average momentum loss of the particles and result in higher average particle velocities near the walls (Fig. 11). For larger particles a reduction in the mean horizontal transport velocity is observed due to wall roughness and accordingly the slip velocity is increasing. This is the result of increasing wall collision frequency and the associated increase of the momentum loss.

The influence of inter-particle collisions on the particle phase mean transport velocity was found to be rather small for the considered range of mass loading. With wall roughness a slight decrease was found due to inter-particle collisions and the involved momentum loss. Somewhat stronger variations of the vertical velocity profiles were observed especially for the smooth wall and the 110 μm particles where inter-particle collisions change the pattern of particle motion considerably (compare Figs. 2 and 3). In this case the particle mean velocity is decreasing near the bottom of the channel (i.e. up to $y/H = 0.2$) with increasing mass loading and hence inter-particle collision frequency (Fig. 12a). In the upper part of the channel an increase of the particle mean velocity is found. This is associated with the enhanced lateral dispersion of the particles and the reduction of the collision frequency with the lower wall. In the case of the rough wall the particle mean velocity changes only slightly with mass loading, especially up to $y/H = 0.7$, but no clear trends are observed (Fig. 12b).

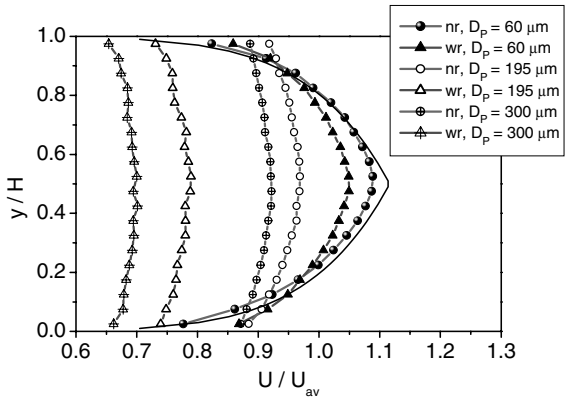

Fig. 11. Vertical profiles of the normalised horizontal component of the particle velocity for different particle diameters, comparison of cases without and with wall roughness including inter-particle collisions ($H = 35$ mm, $\eta = 1.0$, $U_{av} = 18$ m/s, the closed line represents the prescribed gas velocity profile, nr: no wall roughness, wr: with wall roughness).

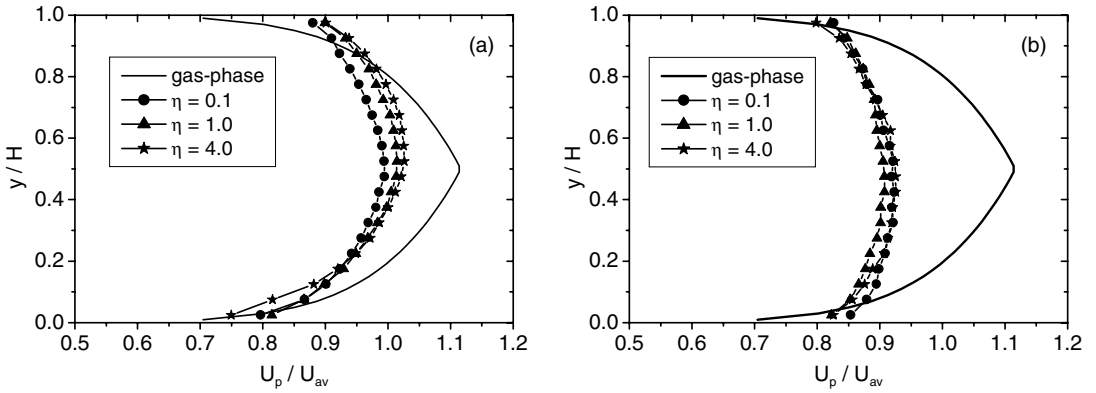

Fig. 12. Vertical profiles of streamwise particle mean velocity in a developed state demonstrating the effect of inter-particle-collisions, (a) without wall roughness, (b) with wall roughness ($H = 35$ mm, $U_{av} = 18$ m/s, $D_p = 110$ μm).

The effect of wall roughness and inter-particle collisions on the particle phase fluctuating velocities have been discussed previously (Sommerfeld, 1995). Therefore, here only one result demonstrating the effect of inter-particle collisions without and with roughness will be shown. For smaller particles (i.e. 60 μm) both components of the fluctuating velocity are generally lower than that of the gas phase if no wall roughness is considered (Fig. 13). The effect of inter-particle collisions without wall roughness is mainly occurring in the lower section of the channel (i.e. up to $y/H \approx 0.7$). For the streamwise component a strong reduction of the fluctuating velocity with increasing mass loading is observed, while the transverse component is enhanced slightly in the region near the bottom wall (i.e. up to $y/H \approx 0.3$). This implies that in this region where the inter-particle collision frequency is high, an isotropisation of the fluctuating behaviour of the particles is occurring due to inter-particle collisions (Fig. 13).

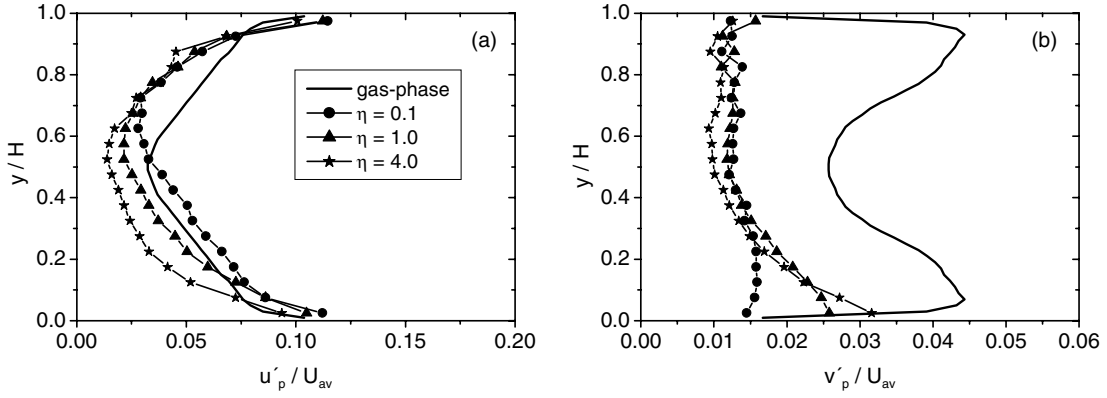

Fig. 13. Vertical profiles of particle velocity fluctuations in a developed state demonstrating the effect of inter-particle-collisions without wall roughness, (a) streamwise component, (b) transverse component ($H = 35$ mm, $U_{av} = 18$ m/s, $D_p = 60$ μm).

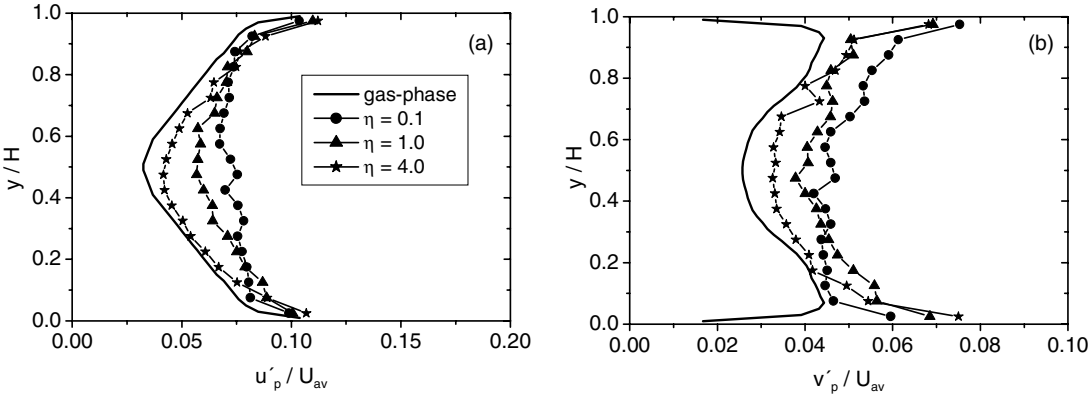

Fig. 14. Vertical profiles of particle velocity fluctuations in a developed state demonstrating the effect of inter-particle-collisions with wall roughness, (a) streamwise component, (b) transverse component ($H = 35$ mm, $U_{av} = 18$ m/s, $D_p = 60$ μm).

For the case of the rough wall and the same particle size (i.e. 60 μm) the fluctuating velocities of the particles become higher than those of the gas phase due to the irregular wall bouncing and the associated strong lateral particle dispersion (Fig. 14). In this case inter-particle collisions cause an overall reduction of both fluctuating components, however that of the streamwise component is somewhat stronger in the core of the channel. This implies a smaller isotropisation of the fluctuating motion compared to the smooth wall and reveals that the fluctuations are mainly governed by wall collisions and have already very similar values before collisions become more important. Hence, inter-particle collisions induce a further equilibration of the fluctuating velocities of the particles (Fig. 14). For larger particles (i.e. 300 μm) it was found that the streamwise component was reduced remarkably and the transverse component remained almost unchanged. These effects will be further analysed in a second contribution (Sommerfeld and Kussin, 2003) where the integral properties of the particle phase will be considered.

4. Conclusion

A detailed analysis of the particle behaviour in a horizontal channel has been presented based on numerical calculations by the Lagrangian approach. It was demonstrated that for small particles wall roughness causes a considerable reduction of wall collision frequency (i.e. increase of wall collision mean free path), whereas a drastic increase of this characteristic value is found for particles with response times larger than about 50 ms. Moreover, wall roughness has an important effect on the horizontal particle mean velocity and the fluctuating components. The particle mean velocity is decreased, while the fluctuating velocities are considerably enhanced, depending on the degree of roughness. Due to the segregation effects (i.e. gravitational settling) regions of high particle concentration develop near the bottom, but inter-particle collisions will cause a lateral dispersion of these particles, both without and with wall roughness. This enhanced dispersion of the particles by collisions also increases the collision probability with the upper wall. Finally it is

also demonstrated that inter-particle collisions cause a redistribution of the particle phase fluctuating motion, namely a decrease of the streamwise component and an enhancement of the lateral component for the smooth wall until an equilibrium is reached. For rough walls this effect is less pronounced, since the particle behaviour is strongly governed by the irregular wall bouncing process and both components are reduced.

For practical design these studies reveal, that for small particles the wall collision frequency is decreasing with increasing mass loading for smooth and rough walls as a result of inter-particle collisions. This might also reduce the possibility of particle degradation during wall impact and pressure loss. In the case of larger particles, wall roughness effects are dominating and a smooth wall will yield lower wall collision frequencies, resulting also in less pressure drop and particle degradation.

In the second part of this analysis integral properties for the particle behaviour in a horizontal channel and information on the angular velocity of the particles will be introduced. Additionally, results for a higher channel will be presented, giving an indication about the scale-up of the findings. Finally, the model calculations will be validated bases on detailed experiments by phase-Doppler anemometry (PDA) for different particle sizes and mass loading.

Acknowledgement

The research project is financially supported by the Deutsche Forschungsgemeinschaft. This support under contract number So 204/12-1 and 2 is gratefully acknowledged.

References

Adam, O., 1960. Untersuchungen über die Vorgänge in feststoffbeladenen Gasströmungen, Forschungsberichte des Landes Nordrhein-Westfalen Westdeutscher Verlag, Köln.

Brauer, H., 1980. Report on investigations on particle movement in straight horizontal tubes, particle/wall collision and erosion of tubes and tube bends. J. Powder Bulk Solids Technol. 4, 3–12.

Burmester De Bessa Ribas, R., Lourenco, L., Riethmuller, M.L., 1980. A kinetic model for gas–particle flow. In: Pneumotransport 5, 5th International Conference on Pneumatic Transport of Solids in Pipes, Paper B2. pp. 99–112.

Cao, J., Ahmadi, G., 1995. Gas–particle two-phase turbulent flow in a vertical duct. Int. J. Multiphase Flow 21, 1203–1228.

Crowe, C.T., Sommerfeld, M., Tsuji, Y., 1998. Fundamentals of gas–particle and gas–droplet flows. CRC Press.

Dennis, S.C.R., Singh, S.N., Ingham, D.B., 1980. The steady flow due to a rotating sphere at low and moderate Reynolds numbers. J. Fluid Mech. 101, 257–279.

Frank, Th., Schade, K.-P., Petrak, D., 1993. Numerical simulation and experimental investigation of a gas–solid two-phase flow in a horizontal channel. Int. J. Multiphase Flow 19, 187–198.

Gore, R.A., Crowe, C.T., 1989. Effect of particle size on modulating turbulent intensity. Int. J. Multiphase Flow 15, 279–285.

Huber, N., Sommerfeld, M., 1994. Characterization of the cross-sectional particle concentration distribution in pneumatic conveying systems. Powder Technol. 79, 191–210.

Huber, N., Sommerfeld, M., 1998. Modelling and numerical calculation of dilute-phase pneumatic conveying in pipe systems. Powder Technol. 99, 90–101.

Kulick, J.D., Fessler, J.R., Eaton, J.K., 1994. Particle response and turbulence modification in fully developed channel flow. J. Fluid Mech. 277, 109–134.

Kussin, J., Sommerfeld, M., 2002. Experimental studies on particle behaviour and turbulence modification in horizontal channel flow with different wall roughness. Exp. Fluids 33, 143–159.

Laufer, J., 1950. Investigation of turbulent flow in a two-dimensional channel. National Advisory Committee for Aeronautics, NACA Technical Note 2123.

Lee, S.L., Durst, F., 1982. On the motion of particles in turbulent duct flows. Int. J. Multiphase Flow 8, 125–146.

Louge, M.Y., Mastorakos, E., Jenkins, J.T., 1991. The role of particle collisions in pneumatic transport. J. Fluid Mech. 231, 345–369.

Lourenco, L., Riethmuller, M.L., Essers, J.-A., 1983. The kinetic model for gas particle flow and its numerical implementation. In: International Conference on the Physical Modelling of Multi-Phase Flow, Coventry, England, April 19–21.

Lun, C.K.K., Liu, H.S., 1997. Numerical simulation of dilute turbulent gas–solid flows in horizontal channels. Int. J. Multiphase Flow 23, 575–605.

Matsumoto, S., Saito, S., 1970. Monte Carlo simulation of horizontal pneumatic conveying based on the rough wall model. J. Chem. Eng. Japan 3, 223–230.

Mei, R., 1992. An approximate expression for the shear lift force on a spherical particle at finite Reynolds number. Int. J. Multiphase Flow 18, 145–147.

Oesterlé, B., 1991. Numerical prediction of particle trajectories in a pipe bend. In: Proceedings of the 5th Workshop on Two-phase Flow Predictions, Erlangen, 1990. Forschungszentrum Jülich, pp. 148–155.

Oesterlé, B., Petitjean, A., 1993. Simulation of particle-to-particle interactions in gas–solid flows. Int. J. Multiphase Flow 19, 199–211.

Oesterlé, B., Bui Dinh, T., 1998. Experiments on the lift of a spinning sphere in a range of intermediate Reynolds numbers. Exp. Fluids 25, 16–22.

Ogawa, S., 1983. On statistical approaches to the dynamics of fully fluidized granular materials. In: Shahinpoor, M. (Ed.), Advances in the Mechanics and Flow of Granular Materials. Trans-Tech, pp. 601–612.

Ottjes, J.A., 1978. Digital simulation of pneumatic particle transport. Chem. Eng. Sci. 33, 783–786.

Rubinow, S.I., Keller, J.B., 1961. The transverse force on spinning sphere moving in a viscous fluid. J. Fluid Mech. 11, 447–459.

Saffman, P.G., 1965. The lift on a small sphere in a shear flow. J. Fluid Mech. 22, 385–400.

Sawatzki, O., 1970. Strömungsfeld um eine rotierend Kugel. Acta Mech. 9, 159–214.

Schlichting, H., 1982. Grenzschicht-Theorie. Verlag G. Braun, Karlsruhe.

Sinclair, J.L., Jackson, R., 1989. Gas–particle flow in a vertical pipe with particle–particle interactions. AIChE J. 35, 1473–1486.

Sommerfeld, M., 1992. Modelling of particle–wall collisions in confined gas–particle flows. Int. J. Multiphase Flows 18, 905–926.

Sommerfeld, M., 1995. The importance of inter-particle collisions in horizontal gas–solid channel flows. In: Stock, D.E. et al. (Eds.), Gas–Particle Flows. In: ASME Fluids Engineering Conference, Hiltons Head, USA, FED-Vol. 228. ASME, pp. 335–345.

Sommerfeld, M., 1996. Modellierung und numerische Berechnung von partikelbeladenen turbulenten Strömungen mit Hilfe des Euler/Lagrange-Verfahrens. Habilitaionsschrift, Universität Erlangen-Nürnberg, Shaker Verlag, Aachen.

Sommerfeld, M., 1998. Modelling and numerical calculation of turbulent gas–solid flows with the Euler/Lagrange approach. KONA (Powder and Particle) 16, 194–206.

Sommerfeld, M., 2000. Theoretical and experimental modelling of particulate flow: overview and fundamentals. Von Karman Institute for Fluid Mechanics, Rhode Saint Genèse, Belgium. Lecture Series No. 2000-6, pp. 1–62.

Sommerfeld, M., 2001. Validation of a Lagrangian modelling approach for inter-particle collisions in homogeneous isotropic turbulence. Int. J. Multiphase Flow 27, 1828–1858.

Sommerfeld, M., Zivkovic, G., 1992. Recent advances in the numerical simulation of pneumatic conveying through pipe systems. In: Hirsch, Ch., Periaux, J., Onate, E. (Eds.), Computational Methods in Applied Science. In: Invited Lectures and Special Technological Sessions of the First European Computational Fluid Dynamics Conference and the First European Conference on Numerical Methods in Engineering, Brussels. pp. 201–212.

Sommerfeld, M., Huber, N., 1999. Experimental analysis and modelling of particle–wall collisions. Int. J. Multiphase Flow 25, 1457–1489.

Sommerfeld, M., Kussin, J., 2003. Analysis of collision effects for gas–particle flow in a horizontal channel: Part II. Integral properties and validation. Int. J. Multiphase Flow, 29, doi:10.1016/S0301-9322(03)00033-8.

Sommerfeld, M., Kohnen, G., Rüger, M., 1993. Some open questions and inconsistencies of Lagrangian Particle dispersion models. In: Ninth Symposium on Turbulent Shear Flows, Kyoto, August 1993 (Paper 15.1).

Tanaka, T., Tsuji, Y., 1991. Numerical simulation of gas–solid two-phase flow in a vertical pipe: on the effect of inter-particle collision. In: Stock, D.E., Tsuji, Y., Jurewicz, J.T., Reeks, M.W., Gautam, M. (Eds.), Gas–Solid Flows. In: FED-Vol. 121. ASME, pp. 123–128.

Tsuji, Y., 1993. Discrete particle simulation of gas–solid flows (from dilute to dense flow). KONA (Powder and Particles) 11, 57–68.

Tsuji, Y., Morikawa, Y., 1978. Computer simulation for the pneumatic transport in pipes with bends. In: Pneumotransport 4, Fourth International Conference on the Pneumatic Transport of Solids in Pipes (Paper B1).

Tsuji, Y., Morikawa, Y., 1982. LFV measurements of an air–solid two-phase flow in a horizontal pipe. J. Fluid Mech. 120, 385–409.

Tsuji, Y., Morikawa, Y., Shiomi, H., 1984. LFV measurements of an air–solid two-phase flow in a verticall pipe. J. Fluid Mech. 139, 417–434.

Tsuji, Y., Oshima, T., Morikawa, Y., 1985. Numerical simulation of pneumatic conveying in a horizontal pipe. KONA 3, 38–51.

Tsuji, Y., Morikawa, Y., Tanaka, T., Nakatsukasa, N., Nakatani, M., 1987. Numerical simulation of gas–solid two-phase flow in a two-dimensional horizontal channel. Int. J. Multiphase Flow 13, 671–684.

Tsuji, Y., Shen, N.Y., Morikawa, Y., 1989. Numerical simulation of gas–solid flows. I: Particle-to-wall collisions. Technology Reports of the Osaka University, vol. 39. pp. 233–241.

Tsuji, Y., Shen, N.Y., Morikawa, Y., 1991. Lagrangian simulation of dilute gas–solid flows in a horizontal pipe. Adv. Powder Technol. 2, 63–81.

Tu, J.Y., Fletcher, C.A.J., 1995. Numerical computation of turbulent gas–solid particle flow in a 90° bend. AIChE Journal 41, 2187–2197.

Varaksin, A.Y., Polezhaev, Y.V., Polyakov, A.F., 1998. Experimental investigation of the effect of solid particles on turbulent flow of air in a pipe. High Temp. 36, 744–752.

Varaksin, A.Yu., Polezhaev, Y.V., Polyakov, A.F., 1999. Effect of the particles concentration on fluctuating velocity of the disperse phase for turbulent pipe flow. In: Turbulence and Shear Flow Phenomena—1, First International Symposium, September 12–15, Santa Barbara, CA.

Wang, Q., Squires, K.D., Chen, M., McLaughlin, J.B., 1997. On the role of lift forces in turbulence simulation of particle deposition. Int. J. Multiphase Flow 23, 749–763.